

## Article

# Changes in Drought Characteristics in the Yellow River Basin during the Carbon-Neutral Period under Low-Emission Scenarios

Xunyu Li <sup>1</sup>, Yang Jiao <sup>1,2,\*</sup>  and Jieyu Liu <sup>1</sup>

<sup>1</sup> School of Hydrology and Water Resources, Nanjing University of Information Science and Technology, Nanjing 210044, China; xyli0925@163.com (X.L.); 202312600007@nuist.edu.cn (J.L.)

<sup>2</sup> Key Laboratory of Hydrometeorological Disaster Mechanism and Warning of Ministry of Water Resources, Nanjing University of Information Science and Technology, Nanjing 210044, China

\* Correspondence: jiaoyang@nuist.edu.cn

**Abstract:** Droughts have a severe impact on the environment and social economy, and predicting their future changes is challenging due to significant uncertainties in climate change and human activities. Many countries have pledged to achieve carbon neutrality to limit global warming; however, few studies have focused on drought changes during the carbon-neutral period. Here, we analyzed the variations in drought characteristics across the Yellow River Basin (YRB) during the carbon-neutral period under two low-emission scenarios from 7 CMIP6 model outputs. The results show that the temperature and precipitation will increase significantly during the 2015–2100 period under both SSP1-1.9 and SSP1-2.6 scenarios. Compared to the historical period (1979–2014), the hydrological drought frequency is projected to decrease by 15.5% (13.0–18.1%), while drought severity is expected to increase by 14.4% (13.2–15.7%) during the carbon-neutral period. Meteorological droughts exhibit a similar changing trend, although the results vary between different regions. In general, more severe hydrological droughts may occur in the southern YRB in the carbon-neutral period under low-emission scenarios. This study has implications for future drought mitigation within the Yellow River Basin.

**Keywords:** drought; carbon-neutral period; the Yellow River Basin; climate change; SSPs; CMIP6



**Citation:** Li, X.; Jiao, Y.; Liu, J.

Changes in Drought Characteristics in the Yellow River Basin during the Carbon-Neutral Period under Low-Emission Scenarios. *Water* **2024**, *16*, 1045. <https://doi.org/10.3390/w16071045>

Academic Editor: Achim A. Beylich

Received: 3 March 2024

Revised: 27 March 2024

Accepted: 2 April 2024

Published: 5 April 2024



**Copyright:** © 2024 by the authors. Licensee MDPI, Basel, Switzerland. This article is an open access article distributed under the terms and conditions of the Creative Commons Attribution (CC BY) license (<https://creativecommons.org/licenses/by/4.0/>).

## 1. Introduction

Extreme hydrometeorological events (e.g., heat waves, storms, floods, and droughts) have attracted increasing attention globally [1–5], and climate change is regarded as the main reason for their frequent occurrence in recent decades [6,7]. As a critical indicator of climate change, the mean global surface temperature in 2011–2020 has increased by 1.09 °C compared to the preindustrial period (1850–1900) according to the Sixth Assessment Report (AR6) released by the Intergovernmental Panel on Climate Change (IPCC) [8]. Furthermore, studies predict that future warming is likely to reach 3.3 to 5.7 °C at the end of the 21st century under high-greenhouse-gas-emission scenarios, showing a continuous warming trend [8]. To limit the level of warming, many countries have pledged to achieve carbon neutrality targets, with China setting a goal of “carbon peaking by 2030 and carbon neutrality by 2060”, aiming at reducing emissions of greenhouse gases such as carbon dioxide (CO<sub>2</sub>) and methane (CH<sub>4</sub>), avoiding irreversible climate impacts, and reducing the risk of extreme events. Nonetheless, extensive work is still needed to assess the spatial-temporal characteristics of hydrometeorological extremes when carbon neutrality targets have been reached because of the complex and heterogeneous interactions between the atmosphere, hydrosphere, and anthroposphere.

Droughts are typically regarded as extreme events characterized by a shortage of water resources and enhanced by reduced precipitation and increased evaporative demand [3,9–11]. The occurrence and development of droughts involve multi-scale water and

energy cycle mechanisms and have severe consequences for the economy and society [12]. Meteorological droughts (the lack of precipitation or moisture) due to climate anomalies may progress into agricultural droughts (the lack of soil moisture), hydrological droughts (the lack of streamflow or runoff), and socioeconomic droughts (the lack of water supply for economic reasons) [13], and further result in vegetation degradation and compound disasters [14]. It is of great importance to monitor, assess, and simulate droughts to reduce their impacts on the environment and social economy; however, the long-term projection of droughts remains a major challenge due to the large uncertainties surrounding future climate change and complex human activities.

Many climate change studies have been conducted on characterizing various types of droughts and quantifying their future changes by applying ensemble simulations based on different socioeconomic development scenarios, which describe different water management policies, urbanization levels, and carbon emissions. A widely used global climate model dataset with comprehensive scenarios is provided by the Coupled Model Intercomparison Project Phase 6 (CMIP6), promoted by the World Climate Research Programme (WCRP). It contains scientific combinations of Representative Concentration Pathways (RCPs) and Shared Socioeconomic Pathways (SSPs) [15], including two low-emission scenarios, SSP1-1.9 and SSP1-2.6, which could achieve carbon neutrality in specific periods in the 21st century [16–18]. The SSP1-1.9 scenario is for global CO<sub>2</sub> emissions to be cut to net zero around 2050, keeping global warming at about 1.5 °C, while the SSP1-2.6 is for global CO<sub>2</sub> emissions to reach net zero after 2050, with the temperature stabilizing at about 1.8 °C and above [8].

At present, studies on drought evolution under different scenarios have attracted the attention of many researchers and have been conducted at both global and regional scales based on CMIP simulations [12,19–27]. Focusing on China, studies show that future drought events will be more frequent and severe with longer durations in the Northwest River Basin and the middle Yangtze River Basin compared to the reference period, and higher emissions signify a greater increase in drought frequency and intensity in the long-term period [24]. Typically, the intensity and duration of drought in the Northwest, Southwest, and Songliao River Basins would increase significantly under all four future scenarios (SSP1-2.6, SSP2-4.5, SSP3-7.0, and SSP5-8.5) [25]. These studies generally focus on predetermined future decades; however, few researchers concentrate on drought changes during periods when specific targets are met, such as the 2 °C global warming level under different SSPs [28,29] and carbon neutrality target under low-emission scenarios [30].

Based on the above discussion, the purpose of this study is to (1) characterize hydrometeorological variables and droughts during the period in which carbon neutrality is met (hereafter “the carbon-neutral period”), and (2) quantify the changes in droughts during the carbon-neutral period compared to a specific historical baseline. Focusing on the Yellow River Basin (YRB) as a testbed, we first established a land surface hydrological model to obtain the historical runoff and then analyzed the spatial–temporal patterns of temperature, precipitation, and runoff from 1979 to 2100 using CMIP6 outputs under the SSP1-1.9 and SSP1-2.6 scenarios. After evaluating and selecting the models, both hydrological and meteorological droughts were identified, characterized, and compared to the baseline period and the carbon-neutral period under the two low-emission scenarios.

## 2. Materials and Methods

### 2.1. Study Area

The Yellow River is the second longest river in China and is located in the mid-latitude area (Figure 1). It flows through arid, semi-arid, and semi-humid areas, with the elevation decreasing from northwest to southeast, and its route contains dense agricultural areas with 107 million inhabitants [31]. The flood season (from July to October) accounts for 60% of the annual runoff, while the dry season (from March to June) accounts for only 10% to 20% [32]. Due to the influence of geographical location and the monsoon climate, the YRB suffers from significant spatio-temporal variations in its water resources and frequent

drought disasters [33,34]. With climate change and the dramatic increase in human water withdrawal and demand, the frequency of extreme droughts in the YRB has increased since the 1980s, posing a great risk to local water resource security as well as energy, food, and ecological security.

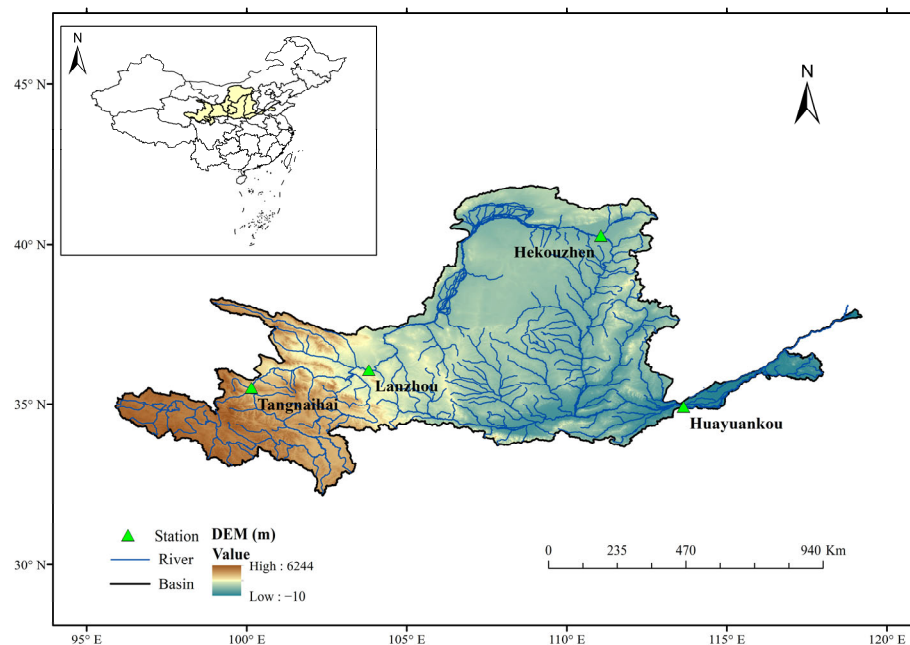


**Figure 1.** Location, elevation, and river networks of the YRB. Four main hydrological stations are indicated as green triangles.

## 2.2. Materials

### 2.2.1. Meteorological Forcings and Streamflow Records

Meteorological forcings (air temperature, surface pressure, humidity, wind speed, shortwave and longwave radiation) during the 1979–2014 period came from the 3-hourly China Meteorological Forcing Dataset (CMFD) at a resolution of 10 km [35]. The precipitation during 1979–2014 came from a gridded daily dataset named CN05.1 with a resolution of  $0.25^\circ$  (about 25 km at the equator), which was constructed for high-resolution climate model validation in China [36]. Another hourly dataset with a higher resolution of 6.25 km was collected from the China Meteorological Administration (CMA) Land Data Assimilation System (CLDAS) for temporal downscaling and bias correction of CN05.1 precipitation by using the quantile mapping method [28]. All meteorological forcings were then resampled to a 5-arc-minute resolution ( $1/12$  degree, about 8 km at the equator) for further model establishment and meteorological drought analysis. Monthly naturalized streamflow records in 1981–2010 at four hydrological stations (Figure 1) were obtained from the Yellow River Conservancy Commission (YRCC) for model evaluation and hydrological drought characterization. These data were estimated by incorporating local human interventions (reservoir operation, agricultural irrigation, domestic water use, etc.) into the monthly observed streamflow data measured at the selected stations.

### 2.2.2. CMIP6 Model Simulations and Carbon-Neutral Periods

All available CMIP6 models that provide total runoff (i.e., the total amount of surface and subsurface runoff), precipitation, and air temperature outputs were chosen (Table 1). Monthly simulations for both the historical (1979–2014) and future (2015–2100) periods were then collected, and two low-carbon-emission scenarios (i.e., SSP1-1.9 and SSP1-2.6) were taken into consideration, under which carbon neutrality can be achieved in the 21st century based on previous studies [7,17,18]. In this study, the carbon-neutral period for the

SSP1-1.9 scenario was set to 2032–2051, and for the SSP1-2.6 scenario was set to 2054–2073, which is consistent with Deng et al. [37]. All CMIP6 model simulations were interpolated to a 5-arc-minute resolution via the bilinear method. The quantile mapping method [28] was also applied to the historical CMIP6-simulated precipitation and temperature to show their biases, and no significant differences in the changing trends between the CMIP6 outputs and historical records were found (details not presented here). Considering that the assumption of a stable cumulative distribution function could hardly hold for the future period, we simply standardized the original CMIP6 outputs for subsequent analyses.

**Table 1.** Basic information on the CMIP6 models used in this study.

Model	Name	Country	Resolution
1	CanESM5	Canada	$2.8^\circ \times 2.8^\circ$
2	CNRM-ESM2-1	France	$1.4^\circ \times 1.4^\circ$
3	EC-Earth3	European Union	$0.7^\circ \times 0.7^\circ$
4	IPSL-CM6A-LR	France	$1.3^\circ \times 2.5^\circ$
5	MIROC6	Japan	$1.4^\circ \times 1.4^\circ$
6	MIROC-ES2L	Japan	$2.8^\circ \times 2.8^\circ$
7	MRI-ESM2-0	Japan	$1.1^\circ \times 1.1^\circ$

### 2.3. Methods

#### 2.3.1. The Conjunctive Surface–Subsurface Process Model (CSSP)

To characterize the spatial–temporal patterns of hydrological droughts in the YRB, it is preferable to identify droughts based on total runoff generated throughout the basin rather than the streamflow concentrated at individual hydrological stations. Due to a lack of reliable runoff data, here we first established a distributed model to accurately reproduce the monthly naturalized streamflow at the four hydrological stations and then utilized the total runoff simulated at each grid as the trusted historical benchmarks. The Conjunctive Surface–Subsurface Process model (CSSP) is a widely used land surface hydrological model that considers various hydrological processes including surface–subsurface water interactions, lateral flow, and vegetation changes [38]. Some studies have applied the CSSP to global and local scales and their results indicate that the model performs satisfactorily in many watersheds for hydrometeorological modeling and forecasting, and is especially suitable for complex terrain and high-resolution simulations [39,40]. In this study, we built a CSSP (version 2) in the YRB at a half-hourly temporal resolution and a 5-arc-minute spatial resolution corresponding to the previously arranged meteorological forcings and CMIP6 model outputs. After verifying the model by using the naturalized streamflow data, a simulation was conducted from 1979 to 2014 and aggregated to obtain gridded monthly total runoff data for further drought identification.

#### 2.3.2. Identification of Hydrological and Meteorological Drought Characteristics

In this study, we chose two standardized indices, the Standardized Runoff Index (SRI) and the Standardized Precipitation Index (SPI), to characterize hydrological and meteorological droughts, respectively. The SRI and SPI were calculated by applying a two-step method [41–44] to gridded precipitation and total runoff data. Taking the SRI as an example, in the first step, the gamma distribution function was applied to fit the total runoff for each month during 1981–2000, and the total runoff in the historical (1979–2014) and future (2015–2100) periods for that month was then standardized to obtain SRI values using the same parameters in the fitted distribution [43,45]. The second step was to identify and characterize hydrological drought events using threshold methods [41,46,47], with  $-0.8$  being chosen as the threshold value, which is equivalent to a 20th percentile of dry conditions. Months with an SRI below  $-0.8$  were considered dry months, and three or more consecutive dry months were considered to indicate the occurrence of a drought event. To characterize the hydrological drought event, two indicators were selected to describe the drought events, i.e., drought frequency (drought events per decade) and drought severity

(time integral of drought indices below the threshold). This method was also applied to the precipitation data to calculate the SPI and meteorological drought characteristics. The flow diagram of this study is shown in Figure 2.

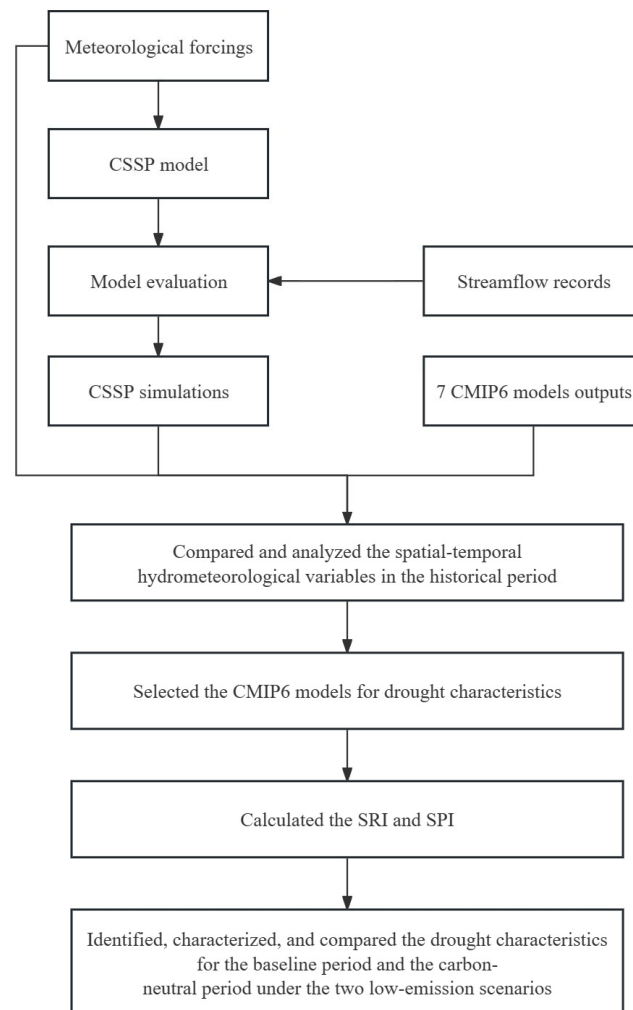


**Figure 2.** The framework and flow diagram of this study.

### 2.3.3. Evaluation Indicators

Four statistical indicators were used to evaluate the model performance and quantify the result comparability in the YRB, i.e., Root Mean Square Error (*RMSE*), Pearson's correlation coefficient (*CC*), Percent bias (*Pbias*), and Kling–Gupta Efficiency (*KGE*). *RMSE* measures the degree of mean deviation between the predicted and true values. *CC* evaluates the linear correlation between two time series. *Pbias* (%) represents the cumulative deviation between the simulated and observed data, with values closer to 0 indicating a better performance. *KGE* reflects the degree of fitting between the simulations and observations, with a value of 1 indicating that the model fits the observations perfectly. The indicators are calculated as follows:

$$RMSE = \sqrt{\frac{1}{n} \sum_{i=1}^n (F_i - O_i)^2} \quad (1)$$

$$CC = \frac{cov(F, O)}{\sigma_F \times \sigma_O} \quad (2)$$

$$Pbias = \frac{\bar{F} - \bar{O}}{\bar{O}} \times 100 \quad (3)$$

$$KGE = 1 - \sqrt{(CC - 1)^2 + (\bar{F}/\bar{O} - 1)^2 + ((\sigma_F/\bar{F})/(\sigma_O/\bar{O}) - 1)^2} \quad (4)$$

where  $F$  refers to the simulation,  $O$  refers to the observation,  $cov$  means the covariance,  $\sigma$  means the standard deviation,  $n$  is the length of the records, and a dash above a variable indicates taking the average value.

### 3. Results

#### 3.1. Model Evaluation

Figure 3 indicates the CSSP's performance by comparing the simulated streamflow to the naturalized records at four major hydrological stations in the YRB during 1981–2010, showing all four statistical indicators. The KGEs reach 0.9, except for the Hekouzhen station with a value of 0.83. The Pbiases for all stations are below 10% and the CCs are greater than 0.9, while the RMSEs show larger biases due to uncertainties when modeling floods. The results generally demonstrate that the CSSP has a good performance in representing monthly streamflow in the YRB, and can provide runoff simulations with sufficient accuracy for later use.

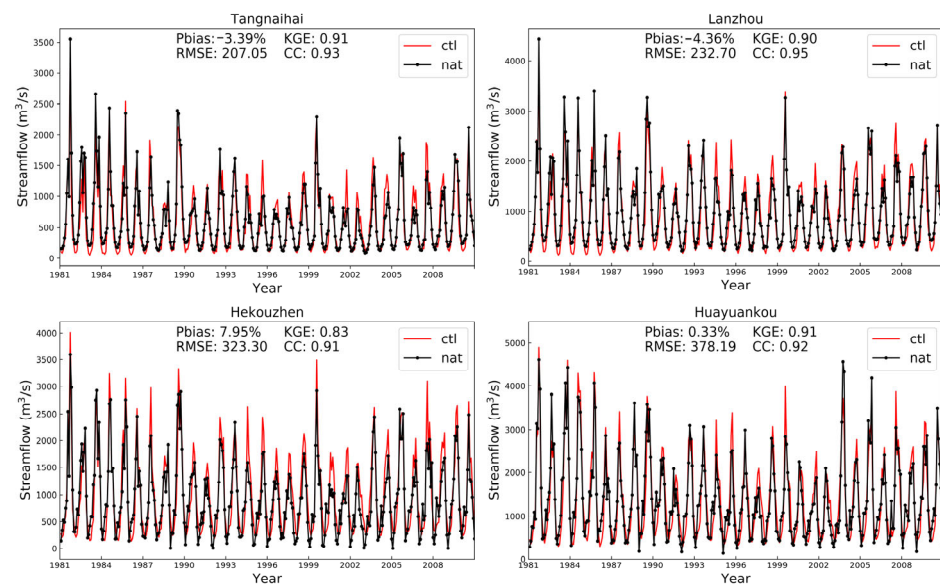


**Figure 3.** Naturalized (nat) and simulated (ctl) monthly streamflow during 1981–2010 at four stations.

#### 3.2. Spatial–Temporal Variations in Precipitation, Temperature, and Total Runoff

##### 3.2.1. Changes in Hydrometeorological Regime

We first calculated the changing trends together with the significance of the basin-averaged annual precipitation, temperature, and total runoff in the historical (1979–2014) and future (2015–2100) periods (Table 2 and Figure 4). For CMIP6 simulations, the multi-model ensemble mean of all seven CMIP6 model outputs (hereafter the “model ensemble”) was figured out for all variables during each period as a reflection of average performance. All calculations were applied to the standardized time series, with changing rates given in units “per decade”, and the confidence level was chosen to be 95%.

**Table 2.** Trends in hydrometeorological variables and hydrological drought frequency in the YRB. Historical CSSP trends were calculated by using the hydrometeorological forcings and simulations of CSSP, and the historical CMIP6, future SSP1-1.9, and SSP1-2.6 results were based on the CMIP6 model ensembles in the corresponding periods. Here, “\*” indicates a significant change at a confidence level of 95% ( $p < 0.05$ ).

Historical (1979–2014) and Future (2015–2100) Scenarios	Changing Trend of Standardized Time Series (per Decade)			
	Temperature	Precipitation	Total Runoff	Drought Frequency
Historical CSSP	0.849 *	0.064	−0.111	0.069
Historical CMIP6	0.671 *	0.113	0.080	0.106
Future SSP1-1.9	0.072 *	0.059 *	0.016	−0.014
Future SSP1-2.6	0.178 *	0.099 *	0.058 *	0.024

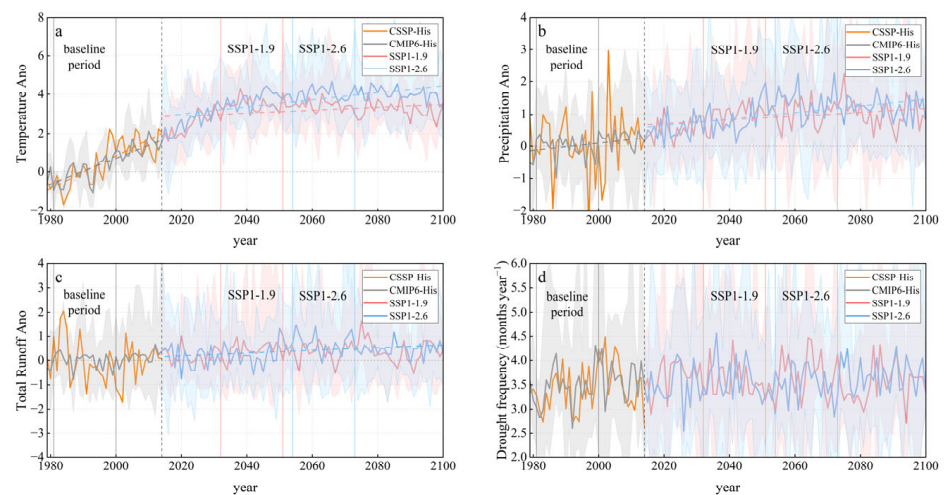


**Figure 4.** Historical and future (SSP1-1.9 and SSP1-2.6) time series of standardized basin-averaged annual (a) temperature, (b) precipitation, (c) total runoff, and (d) hydrological drought frequency (drought months for each year) over the YRB. Shaded areas show the ranges between the maximum and minimum values among CMIP6 model simulations. The dotted lines separate the historical and future periods.

The CSSP historical simulations show that the annual temperature increased significantly by 0.849 per decade, while the precipitation, total runoff, and hydrological drought frequency exhibit no significant changes. Similar results appear in the CMIP6 model ensembles, where the temperature rises at a rate of 0.671 per decade significantly, with no significant changes in the other variables. This means that the model ensemble can capture the historical changes in the hydrometeorological regime; however, the warming trend in the YRB is slightly underestimated. When focusing on future periods, the CMIP6 model-ensimbed temperature and precipitation in both SSP scenarios and the total runoff under SSP1-2.6 increase significantly, and the changing trends are faster for SSP1-2.6 compared to SSP1-1.9. Although not significant, the hydrological drought frequency decreases under the SSP1-1.9 scenario while it increases under the SSP1-2.6 scenario, indicating a large scenario uncertainty when considering extreme events.

A more detailed analysis of hydrometeorological changes for both the historical and future periods is represented in Figure 4. Figure 4a shows that the annual temperature basically peaks in the carbon-neutral period and then gradually declines under the SSP1-1.9 scenario, while the annual temperature under the SSP1-2.6 scenario does not decline very significantly after the carbon-neutral period. The difference in temperature between the two scenarios gradually increases after 2040. In contrast, little difference in the future precipitation and total runoff is found throughout the 21st century, with the precipitation showing an obvious increasing trend for both scenarios. In Figure 4d, it can be seen that the hydrological drought frequency under the SSP1-1.9 scenario decreases at the end of

the 21st century, which corresponds to the results in Table 2. Figure 4 also indicates a large model uncertainty in hydrometeorological simulations among the CMIP6 models.

### 3.2.2. Spatial Patterns of Temperature, Precipitation, and Total Runoff

We then calculated the spatial patterns of the annual mean total runoff, precipitation, and temperature from all CMIP6 models together with the model ensemble in the YRB during the historical period, and compared the results to CSSP meteorological forcings (temperature and precipitation) and simulations (total runoff) based on their correlation coefficients to demonstrate the relevance (Figures 5, 6, and S1). Similar analyses were applied to the carbon-neutral periods under SSP1-1.9 and SSP1-2.6, except that no reliable benchmarks were available for the future (Figures S2 and S3).

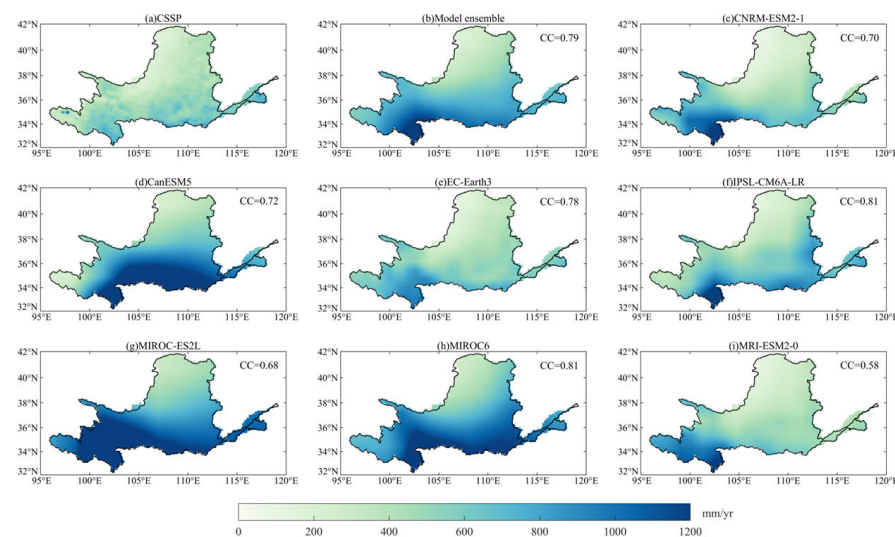


**Figure 5.** Spatial patterns of annual mean precipitation in the YRB during the historical period (1979–2014): (a) the bias-corrected recorded precipitation used as the CSSP meteorological forcings; (b) the CMIP6 model ensemble precipitation; (c–i) the simulated precipitation from each CMIP6 model. The CC marked in the upper-right corners displays the correlation coefficient between the CMIP6 model outputs (including the model ensemble) and the bias-corrected recorded precipitation.

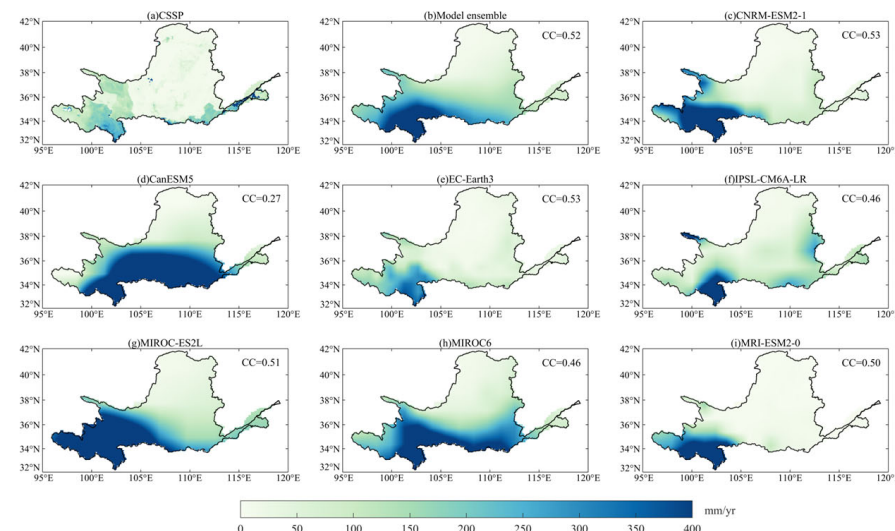


**Figure 6.** The same as Figure 5 but for the simulated annual mean total runoff.

The correlations between the CMIP6 models and CSSP for both the precipitation and temperature are relatively high (0.79 for the model ensemble), indicating that the CMIP6

models simulate well the spatial patterns with the largest precipitation occurring in the southwestern part (river source regions) of the YRB (Figure 5) and the highest temperature existing in the southeastern part (lower reaches) of the YRB (Figure S1). The spatial pattern of the total runoff is consistent with that of the precipitation (Figure 6) because of the semi-arid climate in the YRB; however, most CMIP6 models reasonably represent the runoff relevancy with correlation coefficients lower than 0.50. Generally, CNRM-ESM2-1 and EC-Earth3 perform well in simulating the total runoff, and the model ensemble also provides reliable results in all simulations. The spatial distribution patterns of the total runoff in the carbon-neutral periods under SSP1-1.9 (Figure S2) and SSP1-2.6 (Figure S3) are both consistent with those in the historical period, with a larger runoff generated in the river source regions and in the southern part of the YRB.

### 3.3. Hydrological and Meteorological Drought Characteristics

#### 3.3.1. Hydrological Drought Characteristics

We extracted the hydrological drought characteristics during the historical period based on the gridded total runoff from the CSSP and CMIP6 model simulations, with the CSSP acting as a good estimate of historical droughts. In the historical period, the largest hydrological drought frequency values exist in the upper reaches and southern part of the YRB (Figure 7), and higher drought severity values occur in the upper reaches of the YRB (Figure 8). According to the consistency of the spatial distribution of hydrological drought characteristics, we found that CNRM-ESM2-1 and IPSL-CM6A-LR could provide reasonable results among all CMIP6 models. For the following sections, we then focused on the model ensemble together with these two models to further explore the changes in drought characteristics during the carbon-neutral period under the SSP1-1.9 and SSP1-2.6 scenarios. Although the model ensemble hardly estimates the drought severity, it performs well in simulating the total runoff and drought frequency, indicating that large uncertainties exist in simulating the magnitude and intensity of extreme events.

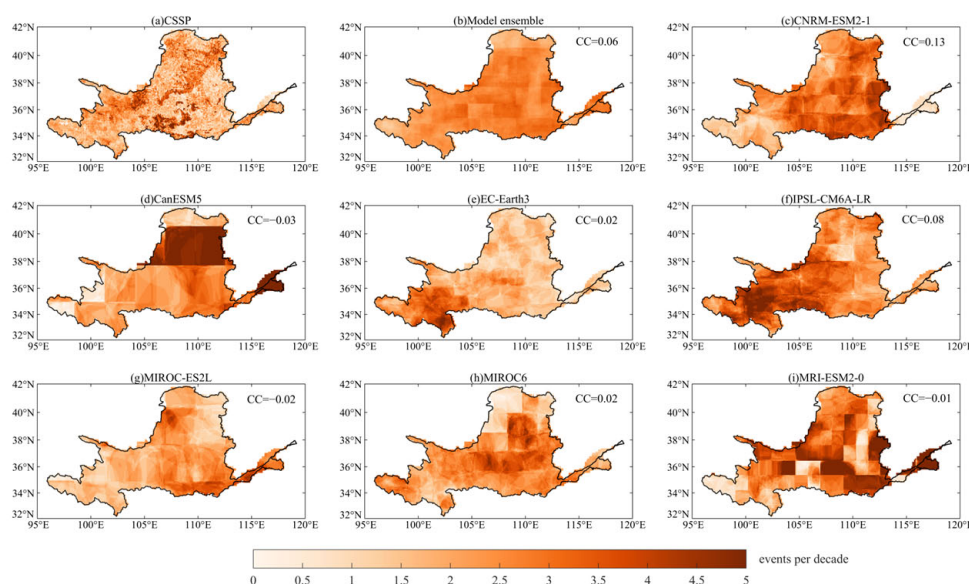


**Figure 7.** Spatial patterns of hydrological drought frequency (events per decade) during the historical period (1979–2014). The CC marked in the upper-right corners depicts the correlation coefficient between the CMIP6 model outputs (including the model ensemble) and the CSSP simulations.

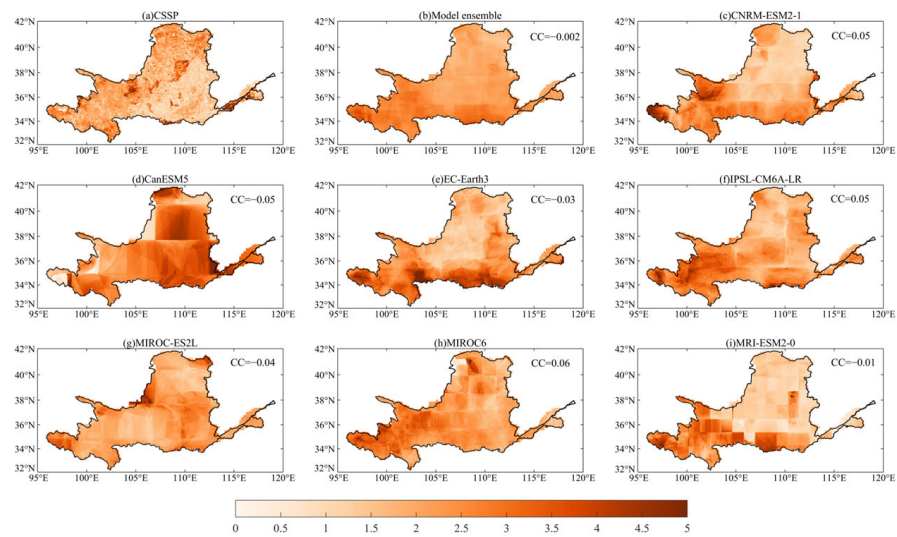


**Figure 8.** The same as Figure 7 but for the hydrological drought severity (unitless).

Figures 9 and 10 show the changes in hydrological drought frequency and severity between the carbon-neutral and historical periods under two low-carbon-emission scenarios based on the model ensemble. Here, “ALL” represents the averaged value in two carbon-neutral periods (i.e., 2032–2051 for SSP1-1.9 and 2054–2073 for SSP1-2.6). Compared to the historical period, the hydrological drought frequency generally decreases with a large decline in the northern YRB. In the southern part, however, the drought frequency increases. The two scenarios show little difference, but SSP1-2.6 demonstrates a greater decrease. The results for CNRM-ESM2-1 and IPSL-CM6A-LR (Figures S4 and S6) also indicate a similar future with fewer drought events when the carbon neutrality target is achieved. On the contrary, the hydrological drought severity will increase in the carbon-neutral periods under both scenarios, with rises mainly occurring in the sources, upper reaches, and southern part of the YRB. Large uncertainties exist when considering the drought severity for each CMIP6 model (Figures S5 and S7). Generally, fewer but more severe hydrological droughts will occur, especially for the southern part of the YRB, during the carbon-neutral period.

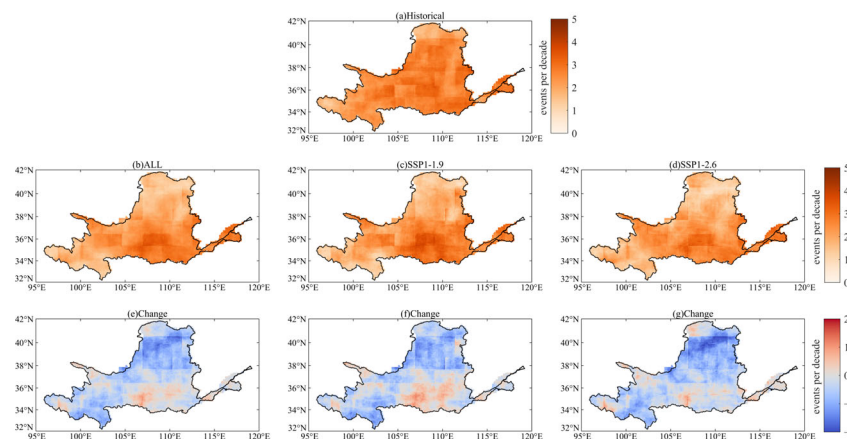


**Figure 9.** Changes in hydrological drought frequency (events per decade) between the carbon-neutral and historical periods (the former minus the latter) under different scenarios. Here, “ALL” was calculated by averaging the characteristic values in carbon-neutral periods under the SSP1-1.9 and SSP1-2.6 scenarios, i.e., 2032–2051 for SSP1-1.9 and 2054–2073 for SSP1-2.6.

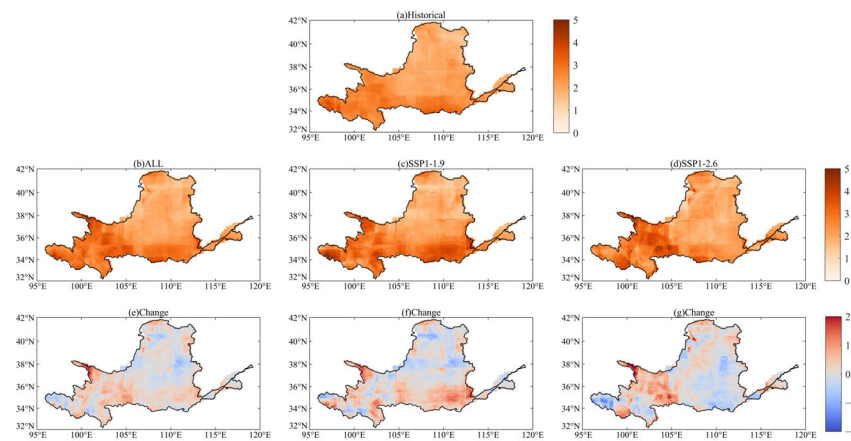


**Figure 10.** The same as Figure 9 but for the hydrological drought severity (unitless).

### 3.3.2. Basin-Averaged Drought Characteristics

We further quantified the basin-averaged hydrological drought frequency and severity in the historical, carbon-neutral, and future periods under both low-emission scenarios (Figure 11). The CMIP6 model ensemble overestimates both the drought frequency and severity in historical periods, partly due to a coarse spatial resolution and an oversimplified hydrological scheme in these climate models. Compared to the historical period, the hydrological drought frequency will decrease in carbon-neutral and future periods. During the carbon-neutral period, the frequency will decrease by 13.0% under SSP1-1.9 and by 18.1% under SSP1-2.6, with an average relative decline of 15.5%. Drought severity is projected to rise by 15.7% under SSP1-1.9 and by 13.2% under SSP1-2.6, resulting in an average gain of 14.4%. When considering the entire future period until the end of the 21st century, the drought frequency will decrease by 12.0% (11.0–13.1%) and the severity will increase by 13.6% (12.6–14.5%).

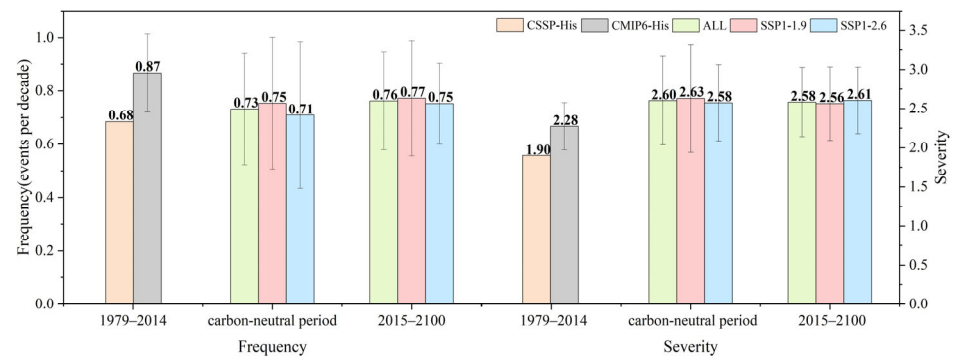


**Figure 11.** Hydrological drought frequency and severity for the historical (1979–2014), carbon-neutral, and future (2015–2100) periods under different scenarios in the YRB. Frequency values are measured on the left vertical axis and severity values are measured on the right vertical axis. “ALL” was calculated by averaging the characteristic values in carbon-neutral periods under the SSP1-1.9 and SSP1-2.6 scenarios, similar to Figure 9.

### 3.3.3. Meteorological Drought Characteristics

The same methods used in Section 3.3.1 were applied to the precipitation in the YRB to determine the meteorological drought characteristics as a reference (Figures 12 and 13). During the historical period, the drought frequency is higher in the central and northern parts of the basin, with meteorological droughts occurring one to two times per decade, while the drought severity is greater in the middle and southern parts of the basin. During the carbon-neutral period, the frequency of meteorological droughts will decrease espe-

cially in the central region, while the drought severity will increase in the northern basin. Compared to SSP1-1.9, SSP1-2.6 is projected to experience a more substantial reduction in drought frequency, which is attributed to a significant rise in future precipitation under this scenario. Generally, meteorological droughts exhibit a similar changing trend to hydrological droughts; however, the variations in spatial patterns differ in their magnitude and critical regions, indicating a complex mechanism behind drought propagation.

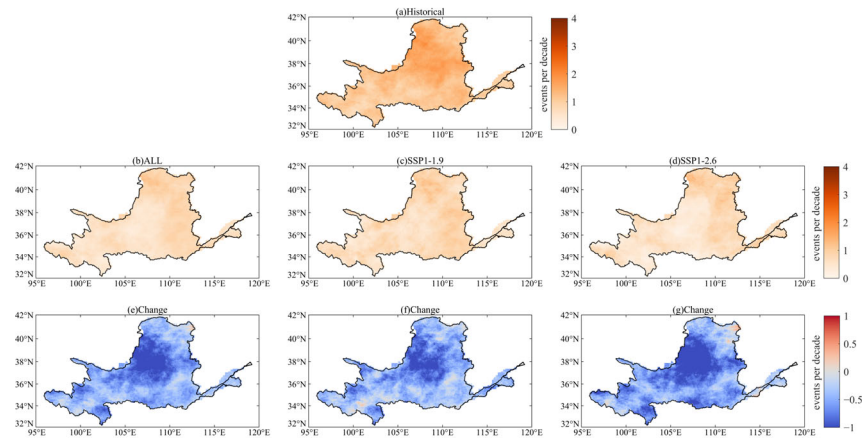


**Figure 12.** The same as Figure 9 but for the meteorological drought frequency (events per decade).

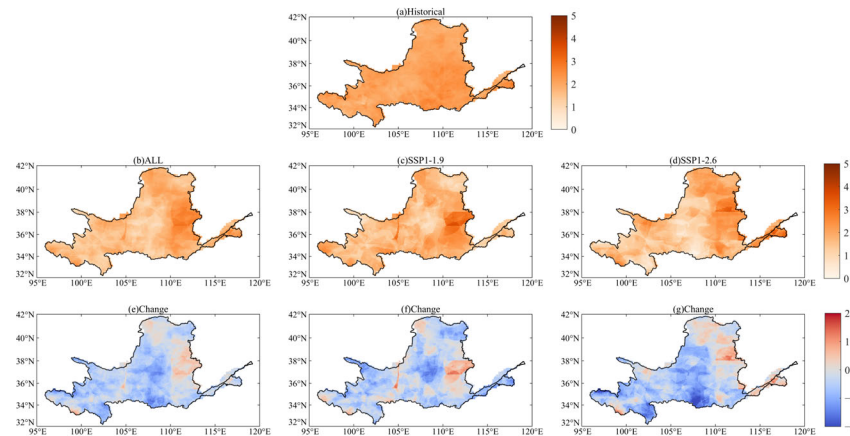


**Figure 13.** The same as Figure 9 but for the meteorological drought severity (unitless).

#### 4. Discussion

In this study, we found that the global warming trend could be effectively managed under two low-emission scenarios, with a decreasing trend in temperature during the carbon-neutral period under the SSP1-1.9 scenario, and a decreasing trend in the middle and the end of the century under the SSP1-2.6 scenario. However, considerable work is still required to quantify the likelihood of extreme disasters. In this study, we found that fewer but more severe hydrological droughts may emerge in the YRB during carbon-neutral periods. This is due to increases in the variability of the total runoff and precipitation from CMIP6 outputs in future periods compared to historical periods, caused by climate change and human activities (see Figure 4), indicating a complex future at the regional scale even if global carbon neutrality targets are achieved. Similar results can be found in other warming-level studies [28,29].

A significant portion of uncertainty arises from the models in the research on climate change predictions. Although we searched all of the CMIP6 models, only seven models were finally chosen due to a lack of available results under SSP1-1.9 and SSP1-2.6 that

could achieve the carbon neutrality targets in the 21st century. Some models (e.g., MIROC-ES2L and CanESM5) perform differently from others due to coarse resolutions, statistical downscaling methods, parameterization schemes, etc. Therefore, a multi-model ensemble is recommended as it can help mitigate the deviation of an individual model to some extent and is used as a compromise solution in predicting future climate change [48–50]. In this study, we calculated the arithmetic average of all seven CMIP6 models and found that they could capture drought frequency well but underperformed in drought severity. Many studies use different weighted averaging methods instead of simple arithmetic averaging, resulting in different model ensembles [51–56]. Here, we also utilized a weighted averaging method and selected the inverse of the RMSE of total runoff during the historical period as the weight for each CMIP6 model to prioritize assigning a higher weight to the more suitable model. As shown in Figure S8, the weighted average model ensemble demonstrated a similar performance to the previous results, suggesting that the performance of the model ensemble is mainly determined by the large model uncertainties rather than the ensemble averaging method used in this study.

The threshold value in the two-step method is crucial for identifying droughts as it signifies different conditions such as mild, moderate, and severe droughts. Different thresholds could lead to variations in drought characteristics. In addition, this study was conducted on a monthly scale, which corresponds to seasonal droughts. Further evaluation work is necessary when considering other types of droughts at sub-seasonal or even weekly timescales [57].

## 5. Conclusions

In this study, based on simulations from the CSSP and CMIP6 models under two low-emission scenarios, SSP1-1.9 and SSP1-2.6, we analyzed the spatial patterns of the annual mean temperature, precipitation, and total runoff in the historical period (1979–2014), carbon-neutral period (2032–2051 for SSP1-1.9 and 2054–2073 for SSP1-2.6), and future period (2015–2100) in the Yellow River Basin. After extracting the drought characteristics by calculating the Standardized Runoff Index (SRI) and Standardized Precipitation Index (SPI) in all periods, we analyzed the changes in hydrological and meteorological drought characteristics between the carbon-neutral period and the historical period. The main results are listed as follows:

1. The CMIP6 model ensemble mean can capture the historical changes well, while the warming trend in the YRB is slightly underestimated. During the future period, the CMIP6 model-enssembled temperature and precipitation in both SSP scenarios and the total runoff under SSP1-2.6 increase significantly, and the changing trends are faster for SSP1-2.6 compared to SSP1-1.9. Although not significant, the hydrological drought frequency decreases under SSP1-1.9, while it increases under SSP1-2.6.
2. The CMIP6 model ensemble overestimates both the drought frequency and severity in historical periods. In carbon-neutral periods, the hydrological drought frequency generally decreases, with a large decline in the northern YRB, while the drought severity will increase under both scenarios, with rises mainly in the sources, upper reaches, and southern part of the YRB, compared to historical periods. Generally, the hydrological drought frequency will decrease by 15.5% (13.0–18.1%), and the drought severity is projected to rise by 14.4% (13.2–15.7%) in carbon-neutral periods.
3. Meteorological droughts exhibit a similar changing trend to hydrological droughts during the carbon-neutral period; however, the variations in spatial patterns differ in their magnitude and critical regions. The frequency of meteorological droughts will decrease, especially in the central region, while the drought severity will increase in the northern basin. SSP1-2.6 is projected to experience a more substantial reduction in drought frequency compared to SSP1-1.9.

Generally, this study enhances the understanding of future drought conditions in the Yellow River Basin, suggesting that more severe hydrological droughts may occur, and

these findings have implications for water resource management and drought mitigation during the carbon-neutral period.

**Supplementary Materials:** The following supporting information can be downloaded at <https://www.mdpi.com/xxx/s1>. Figure S1: Spatial distribution of annual mean temperature in the Yellow River Basin (YRB) during the historical period (1979–2014). CC marked in the upper-right corner means the correlation coefficient between CMIP6 model outputs (including the model ensemble) and the CSSP hydrometeorological forcings; Figure S2: Spatial distribution of annual mean total runoff in the YRB under the SSP1-1.9 scenario during the carbon-neutral period (2032–2051); Figure S3: Spatial distribution of annual mean total runoff in the YRB under the SSP1-2.6 scenario during the carbon-neutral period (2054–2073); Figure S4: Changes in hydrological drought frequency of IPSL-CM6A-LR between the carbon-neutral and historical periods (the former minus the latter) under “ALL”, SSP1-1.9, and SSP1-2.6 scenarios. “ALL” is calculated by averaging the characteristic values in 2032–2051 under SSP1-1.9 and 2054–2073 under SSP1-2.6; Figure S5: The same as Figure S4, but for drought severity; Figure S6: The same as Figure S4, but for drought frequency of CNRM-ESM2-1; Figure S7: The same as Figure S4, but for drought severity of CNRM-ESM2-1; Figure S8: Spatial patterns of (a,b) hydrological drought frequency (events per decade) and (c,d) drought severity during the historical period (1979–2014). CC marked in the upper-right corner means the correlation coefficient between the weighted average model ensemble and the CSSP simulations.

**Author Contributions:** Conceptualization, X.L. and Y.J.; methodology, Y.J.; formal analysis, X.L.; writing—original draft, X.L.; writing—review and editing, Y.J.; data curation, J.L.; funding acquisition, Y.J. All authors have read and agreed to the published version of the manuscript.

**Funding:** This research was funded by the National Natural Science Foundation of China (grants no. 41901035 and U21A2021).

**Data Availability Statement:** The CMFD data can be downloaded at the website of A Big Earth Data Platform for Three Poles (<https://poles.tpdc.ac.cn/en/data/8028b944-daaa-4511-8769-965612652c49/>). The CLDAS dataset can be found at the website of China Meteorological Data Service Centre (<https://data.cma.cn/en>). CMIP6 simulations used in this study were provided by the World Climate Research Programme’s Working Group on Coupled Modeling (<https://esgf-data.dkrz.de/projects/cmip6-dkrz/>).

**Acknowledgments:** We would like to thank the editor and four anonymous reviewers for their helpful comments. We acknowledge the High Performance Computing Center of Nanjing University of Information Science & Technology for their support of this work.

**Conflicts of Interest:** The authors declare no conflicts of interest.

## References

1. Russo, S.; Dosio, A.; Graversen, R.G.; Sillmann, J.; Carrao, H.; Dunbar, M.B.; Singleton, A.; Montagna, P.; Barbola, P.; Vogt, J.V. Magnitude of Extreme Heat Waves in Present Climate and Their Projection in a Warming World. *J. Geophys. Res. Atmos.* **2014**, *119*. [[CrossRef](#)]
2. Wang, X.; Zhao, C.; Müller, C.; Wang, C.; Ciais, P.; Janssens, I.; Peñuelas, J.; Asseng, S.; Li, T.; Elliott, J.; et al. Emergent Constraint on Crop Yield Response to Warmer Temperature from Field Experiments. *Nat. Sustain.* **2020**, *3*, 908–916. [[CrossRef](#)]
3. Dai, A. Increasing Drought under Global Warming in Observations and Models. *Nat. Clim. Chang.* **2013**, *3*, 52–58. [[CrossRef](#)]
4. Trenberth, K.E.; Dai, A.; Van Der Schrier, G.; Jones, P.D.; Barichivich, J.; Briffa, K.R.; Sheffield, J. Global Warming and Changes in Drought. *Nat. Clim. Chang.* **2014**, *4*, 17–22. [[CrossRef](#)]
5. Donat, M.G.; Lowry, A.L.; Alexander, L.V.; O’Gorman, P.A.; Maher, N. More Extreme Precipitation in the World’s Dry and Wet Regions. *Nat. Clim. Chang.* **2016**, *6*, 508–513. [[CrossRef](#)]
6. Degefu, M.A.; Bewket, W. Variability and Trends in Rainfall Amount and Extreme Event Indices in the Omo-Ghibe River Basin, Ethiopia. *Reg. Environ. Chang.* **2014**, *14*, 799–810. [[CrossRef](#)]
7. Gaffin, S.R.; Rosenzweig, C.; Xing, X.; Yetman, G. Downscaling and Geo-Spatial Gridding of Socio-Economic Projections from the IPCC Special Report on Emissions Scenarios (SRES). *Glob. Environ. Chang.* **2004**, *14*, 105–123. [[CrossRef](#)]
8. Climate Change 2021: The Physical Science Basis. In *Contribution of Working Group I to the Sixth Assessment Report of the Intergovernmental Panel on Climate Change*; Cambridge University Press: Cambridge, UK; New York, NY, USA, 2021; pp. 33–144.
9. Huang, J.; Zhai, J.; Jiang, T.; Wang, Y.; Li, X.; Wang, R.; Xiong, M.; Su, B.; Fischer, T. Analysis of Future Drought Characteristics in China Using the Regional Climate Model CCLM. *Clim. Dynam.* **2018**, *50*, 507–525. [[CrossRef](#)]

10. Su, B.; Huang, J.; Fischer, T.; Wang, Y.; Kundzewicz, Z.W.; Zhai, J.; Sun, H.; Wang, A.; Zeng, X.; Wang, G.; et al. Drought Losses in China Might Double between the 1.5 °C and 2.0 °C Warming. *Proc. Natl. Acad. Sci. USA* **2018**, *115*, 10600–10605. [[CrossRef](#)]
11. Zhai, J.; Huang, J.; Su, B.; Cao, L.; Wang, Y.; Jiang, T.; Fischer, T. Intensity–Area–Duration Analysis of Droughts in China 1960–2013. *Clim. Dynam.* **2017**, *48*, 151–168. [[CrossRef](#)]
12. Yao, N.; Li, L.; Feng, P.; Feng, H.; Li Liu, D.; Liu, Y.; Jiang, K.; Hu, X.; Li, Y. Projections of Drought Characteristics in China Based on a Standardized Precipitation and Evapotranspiration Index and Multiple GCMs. *Sci. Total Environ.* **2020**, *704*, 135245. [[CrossRef](#)] [[PubMed](#)]
13. Hao, Z.; Singh, V.P. Drought Characterization from a Multivariate Perspective: A Review. *J. Hydrol.* **2015**, *527*, 668–678. [[CrossRef](#)]
14. AghaKouchak, A.; Chiang, F.; Huning, L.S.; Love, C.A.; Mallakpour, I.; Mazdiyasn, O.; Moftakhari, H.; Papalexiou, S.M.; Ragno, E.; Sadegh, M. Climate Extremes and Compound Hazards in a Warming World. *Annu. Rev. Earth Planet Sci.* **2020**, *48*, 519–548. [[CrossRef](#)]
15. Jiang, T.; Lü, Y.; Huang, J.; Wang, Y.; Su, B.; Tao, H. New Scenarios of CMIP6 Model (SSP-RCP) and Its Application in the Huaihe River Basin. *Adv. Meteorol. Sci. Technol.* **2020**, *10*, 102–109. [[CrossRef](#)]
16. Gidden, M.J.; Riahi, K.; Smith, S.J.; Fujimori, S.; Luderer, G.; Kriegler, E.; Van Vuuren, D.P.; Van Den Berg, M.; Feng, L.; Klein, D.; et al. Global Emissions Pathways under Different Socioeconomic Scenarios for Use in CMIP6: A Dataset of Harmonized Emissions Trajectories through the End of the Century. *Geosci. Model Dev.* **2019**, *12*, 1443–1475. [[CrossRef](#)]
17. O’Neill, B.C.; Tebaldi, C.; Van Vuuren, D.P.; Eyring, V.; Friedlingstein, P.; Hurtt, G.; Knutti, R.; Kriegler, E.; Lamarque, J.-F.; Lowe, J.; et al. The Scenario Model Intercomparison Project (ScenarioMIP) for CMIP6. *Geosci. Model Dev.* **2016**, *9*, 3461–3482. [[CrossRef](#)]
18. Tebaldi, C.; Debeire, K.; Eyring, V.; Fischer, E.; Fyfe, J.; Friedlingstein, P.; Knutti, R.; Lowe, J.; O’Neill, B.; Sanderson, B.; et al. Climate Model Projections from the Scenario Model Intercomparison Project (ScenarioMIP) of CMIP6. *Earth Syst. Dynam.* **2021**, *12*, 253–293. [[CrossRef](#)]
19. Wang, Z.; Zhong, R.; Lai, C.; Zeng, Z.; Lian, Y.; Bai, X. Climate Change Enhances the Severity and Variability of Drought in the Pearl River Basin in South China in the 21st Century. *Agr. For. Meteorol.* **2018**, *249*, 149–162. [[CrossRef](#)]
20. Mondal, S.K.; Huang, J.; Wang, Y.; Su, B.; Zhai, J.; Tao, H.; Wang, G.; Fischer, T.; Wen, S.; Jiang, T. Doubling of the Population Exposed to Drought over South Asia: CMIP6 Multi-Model-Based Analysis. *Sci. Total Environ.* **2021**, *771*, 145186. [[CrossRef](#)]
21. Cook, B.I.; Mankin, J.S.; Marvel, K.; Williams, A.P.; Smerdon, J.E.; Anchukaitis, K.J. Twenty-First Century Drought Projections in the CMIP6 Forcing Scenarios. *Earth’s Future* **2020**, *8*, e2019EF001461. [[CrossRef](#)]
22. Ukkola, A.M.; De Kauwe, M.G.; Roderick, M.L.; Abramowitz, G.; Pitman, A.J. Robust Future Changes in Meteorological Drought in CMIP6 Projections Despite Uncertainty in Precipitation. *Geophys. Res. Lett.* **2020**, *47*, e2020GL087820. [[CrossRef](#)]
23. Zhai, J.; Mondal, S.K.; Fischer, T.; Wang, Y.; Su, B.; Huang, J.; Tao, H.; Wang, G.; Ullah, W.; Uddin, M.J. Future Drought Characteristics through a Multi-Model Ensemble from CMIP6 over South Asia. *Atmos. Res.* **2020**, *246*, 105111. [[CrossRef](#)]
24. Su, B.; Huang, J.; Mondal, S.K.; Zhai, J.; Wang, Y.; Wen, S.; Gao, M.; Lv, Y.; Jiang, S.; Jiang, T.; et al. Insight from CMIP6 SSP-RCP Scenarios for Future Drought Characteristics in China. *Atmos. Res.* **2021**, *250*, 105375. [[CrossRef](#)]
25. Zhang, M.; Yang, X.; Pan, M.; Zhang, L.; Fang, X.; Sheffield, J. Spatio-Temporal Characteristics and Driving Factors of the Meteorological Drought across China Based on CMIP6. *Hydrol. Res.* **2023**, *54*, 382–400. [[CrossRef](#)]
26. Xu, F.; Bento, V.A.; Qu, Y.; Wang, Q. Projections of Global Drought and Their Climate Drivers Using CMIP6 Global Climate Models. *Water* **2023**, *15*, 2272. [[CrossRef](#)]
27. Afsari, R.; Nazari-Sharabian, M.; Hosseini, A.; Karakouzian, M. A CMIP6 Multi-Model Analysis of the Impact of Climate Change on Severe Meteorological Droughts through Multiple Drought Indices—Case Study of Iran’s Metropolises. *Water* **2024**, *16*, 711. [[CrossRef](#)]
28. Jiao, Y.; Yuan, X. More Severe Hydrological Drought Events Emerge at Different Warming Levels over the Wudinghe Watershed in Northern China. *Hydrol. Earth Syst. Sci.* **2019**, *23*, 621–635. [[CrossRef](#)]
29. Chen, S.; Yuan, X. CMIP6 Projects Less Frequent Seasonal Soil Moisture Droughts over China in Response to Different Warming Levels. *Environ. Res. Lett.* **2021**, *16*, 044053. [[CrossRef](#)]
30. Li, C.; Raj Kattel, G.; Zhang, J.; Shang, Y.; Gnyawali, K.R.; Zhang, F.; Miao, L. Slightly Enhanced Drought in the Yellow River Basin under Future Warming Scenarios. *Atmos. Res.* **2022**, *280*, 106423. [[CrossRef](#)]
31. Piao, S.; Ciais, P.; Huang, Y.; Shen, Z.; Peng, S.; Li, J.; Zhou, L.; Liu, H.; Ma, Y.; Ding, Y.; et al. The Impacts of Climate Change on Water Resources and Agriculture in China. *Nature* **2010**, *467*, 43–51. [[CrossRef](#)]
32. Yin, Z.; Otlé, C.; Ciais, P.; Zhou, F.; Wang, X.; Jan, P.; Dumas, P.; Peng, S.; Li, L.; Zhou, X.; et al. Irrigation, Damming, and Streamflow Fluctuations of the Yellow River. *Hydrol. Earth Syst. Sci.* **2021**, *25*, 1133–1150. [[CrossRef](#)]
33. Omer, A. Water Scarcity in the Yellow River Basin under Future Climate Change and Human Activities. *Sci. Total Environ.* **2020**, *749*, 141446. [[CrossRef](#)] [[PubMed](#)]
34. Wang, F.; Wang, Z.; Yang, H.; Zhao, Y. Study of the Temporal and Spatial Patterns of Drought in the Yellow River Basin Based on SPEI. *Sci. China Earth Sci.* **2018**, *61*, 1098–1111. [[CrossRef](#)]
35. He, J.; Yang, K.; Tang, W.; Lu, H.; Qin, J.; Chen, Y.; Li, X. The first highresolution meteorological forcing dataset for land process studies over China. *Sci. Data* **2020**, *7*, 25. [[CrossRef](#)] [[PubMed](#)]
36. Wu, J.; Gao, X. A gridded daily observation dataset over China region and comparison with the other datasets. *Chin. J. Geophys.* **2013**, *56*, 1102–1111. [[CrossRef](#)]

37. Deng, L.; Zhu, H.; Jiang, Z. Projection of climate change in China under carbon neutral scenarios. *Trans. Atmos. Sci.* **2022**, *45*, 364–375. [[CrossRef](#)]
38. Yuan, X.; Ji, P.; Wang, L.; Liang, X.-Z.; Yang, K.; Ye, A.; Su, Z.; Wen, J. High-Resolution Land Surface Modeling of Hydrological Changes Over the Sanjiangyuan Region in the Eastern Tibetan Plateau: 1. Model Development and Evaluation. *J. Adv. Model. Earth Syst.* **2018**, *10*, 2806–2828. [[CrossRef](#)]
39. Ji, P.; Yuan, X.; Jiao, Y. Future Hydrological Drought Changes over the Upper Yellow River Basin: The Role of Climate Change, Land Cover Change and Reservoir Operation. *J. Hydrol.* **2023**, *617*, 129128. [[CrossRef](#)]
40. Ji, P.; Yuan, X.; Shi, C.; Jiang, L.; Wang, G.; Yang, K. A Long-Term Simulation of Land Surface Conditions at High Resolution over Continental China. *J. Hydrometeorol.* **2023**, *24*, 285–314. [[CrossRef](#)]
41. Lorenzo-Lacruz, J.; Morán-Tejeda, E.; Vicente-Serrano, S.M.; López-Moreno, J.I. Streamflow Droughts in the Iberian Peninsula between 1945 and 2005: Spatial and Temporal Patterns. *Hydrol. Earth Syst. Sci.* **2013**, *17*, 119–134. [[CrossRef](#)]
42. Ma, F.; Yuan, X.; Ye, A. Seasonal Drought Predictability and Forecast Skill over China. *J. Geophys. Res. Atmos.* **2015**, *120*, 8264–8275. [[CrossRef](#)]
43. Yuan, X.; Zhang, M.; Wang, L.; Zhou, T. Understanding and Seasonal Forecasting of Hydrological Drought in the Anthropocene. *Hydrol. Earth Syst. Sci.* **2017**, *21*, 5477–5492. [[CrossRef](#)]
44. Tao, Y.; Meng, E.; Huang, Q. Spatiotemporal Changes and Hazard Assessment of Hydrological Drought in China Using Big Data. *Water* **2023**, *16*, 106. [[CrossRef](#)]
45. Vicente-Serrano, S.M.; López-Moreno, J.I.; Beguería, S.; Lorenzo-Lacruz, J.; Azorin-Molina, C.; Morán-Tejeda, E. Accurate Computation of a Streamflow Drought Index. *J. Hydrol. Eng.* **2012**, *17*, 318–332. [[CrossRef](#)]
46. Yuan, X.; Wood, E.F. Multimodel Seasonal Forecasting of Global Drought Onset. *Geophys. Res. Lett.* **2013**, *40*, 4900–4905. [[CrossRef](#)]
47. Hydrological Drought Severity Explained by Climate and Catchment Characteristics. *J. Hydrol.* **2015**, *526*, 3–14. [[CrossRef](#)]
48. Zhu, H.; Jiang, Z.; Li, L. Projection of Climate Extremes in China, an Incremental Exercise from CMIP5 to CMIP6. *Sci. Bull.* **2021**, *66*, 2528–2537. [[CrossRef](#)] [[PubMed](#)]
49. Zhou, B.; Wen, Q.H.; Xu, Y.; Song, L.; Zhang, X. Projected Changes in Temperature and Precipitation Extremes in China by the CMIP5 Multimodel Ensembles. *J. Clim.* **2014**, *27*, 6591–6611. [[CrossRef](#)]
50. Knutti, R.; Furrer, R.; Tebaldi, C.; Cermak, J.; Meehl, G.A. Challenges in Combining Projections from Multiple Climate Models. *J. Clim.* **2010**, *23*, 2739–2758. [[CrossRef](#)]
51. Chen, W.; Jiang, Z.; Li, L. Probabilistic Projections of Climate Change over China under the SRES A1B Scenario Using 28 AOGCMs. *J. Clim.* **2011**, *24*, 4741–4756. [[CrossRef](#)]
52. Giorgi, F.; Mearns, L.O. Probability of Regional Climate Change Based on the Reliability Ensemble Averaging (REA) Method. *Geophys. Res. Lett.* **2003**, *30*, 1629. [[CrossRef](#)]
53. Li, W.; Jiang, Z.; Xu, J.; Li, L. Extreme Precipitation Indices over China in CMIP5 Models. Part II: Probabilistic Projection. *J. Clim.* **2016**, *29*, 8989–9004. [[CrossRef](#)]
54. Li, T.; Jiang, Z.; Zhao, L.; Li, L. Multi-Model Ensemble Projection of Precipitation Changes over China under Global Warming of 1.5 and 2 °C with Consideration of Model Performance and Independence. *J. Meteorol. Res.* **2021**, *35*, 184–197. [[CrossRef](#)]
55. Knutti, R.; Sedláček, J.; Sanderson, B.M.; Lorenz, R.; Fischer, E.M.; Eyring, V. A Climate Model Projection Weighting Scheme Accounting for Performance and Interdependence. *Geophys. Res. Lett.* **2017**, *44*, 1909–1918. [[CrossRef](#)]
56. Giorgi, F.; Mearns, L.O. Calculation of Average, Uncertainty Range, and Reliability of Regional Climate Changes from AOGCM Simulations via the “Reliability Ensemble Averaging” (REA) Method. *J. Clim.* **2002**, *15*, 1141–1158. [[CrossRef](#)]
57. Yuan, X.; Wang, Y.; Ji, P.; Wu, P.; Sheffield, J.; Otkin, J.A. A Global Transition to Flash Droughts under Climate Change. *Science* **2023**, *380*, 187–191. [[CrossRef](#)]

**Disclaimer/Publisher’s Note:** The statements, opinions and data contained in all publications are solely those of the individual author(s) and contributor(s) and not of MDPI and/or the editor(s). MDPI and/or the editor(s) disclaim responsibility for any injury to people or property resulting from any ideas, methods, instructions or products referred to in the content.